

Commute Graph Neural Networks

Wei Zhuo

Shenzhen Campus of Sun Yat-sen University
zhuow5@mail2.sysu.edu.cn

Guang Tan

Shenzhen Campus of Sun Yat-sen University
tanguang@mail.sysu.edu.cn

Abstract

Graph Neural Networks (GNNs) have shown remarkable success in learning from graph-structured data. However, their application to directed graphs (digraphs) presents unique challenges, primarily due to the inherent asymmetry in node relationships. Traditional GNNs are adept at capturing unidirectional relations but fall short in encoding the mutual path dependencies between nodes, such as asymmetrical shortest paths typically found in digraphs. Recognizing this gap, we introduce Commute Graph Neural Networks (CGNN), an approach that seamlessly integrates node-wise commute time into the message passing scheme. The cornerstone of CGNN is an efficient method for computing commute time using a newly formulated digraph Laplacian. Commute time information is then integrated into the neighborhood aggregation process, with neighbor contributions weighted according to their respective commute time to the central node in each layer. It enables CGNN to directly capture the mutual, asymmetric relationships in digraphs.

1 Introduction

Directed graphs (digraphs) are widely employed to model relational structures in diverse domains, such as social networks (Cross et al., 2001) and recommendation systems (Qiu et al., 2020). Recently, the advances of graph neural networks (GNNs) have inspired various attempts to adopt GNNs for analyzing digraphs (Tong et al., 2020a,b, 2021; Zhang et al., 2021; Rossi et al., 2023; Geisler et al., 2023). The essence of GNN-based digraph analysis lies in utilizing GNNs to learn expressive node representations that encode edge direction information.

To achieve this, modern digraph neural networks are designed to integrate edge direction information into the message passing process by distinguishing between incoming and outgoing edges. This distinction enables the central node to learn directionally discriminative information from its neighbors. As illustrated in the digraph of Fig. 1, given a central node v_i , a 1-layer digraph neural network can aggregate messages from v_i 's incoming neighbor v_m and outgoing neighbor v_j , and simultaneously capture edge directions by applying direction-specific aggregation functions (Rossi et al., 2023), or by predefining edge-specific weights (Zhang et al., 2021; Tong et al., 2020b).

Despite the advancements, current digraph neural networks primarily capture unidirectional¹ relationships between nodes, neglecting the complexity arising from path asymmetry. For instance, a k -layer GNN aggregates the neighbors within the shortest path k for the central node. If the graph is undirected, the shortest path between any two nodes is symmetric, as shown in the undirected graph of Fig. 1. This symmetry simplifies the representation of node relationships, implying that if the SPDs from one node to two other nodes are identical, then the SPDs from these two nodes back to the source node must also be the same. Conversely, such symmetry is absent in digraphs. Considering the digraph in Fig. 1, the shortest paths between v_i and v_j are asymmetric. Therefore, although v_j and v_k

¹'unidirectional' refers to relationships in digraphs where edges have a specific direction from one node to another.

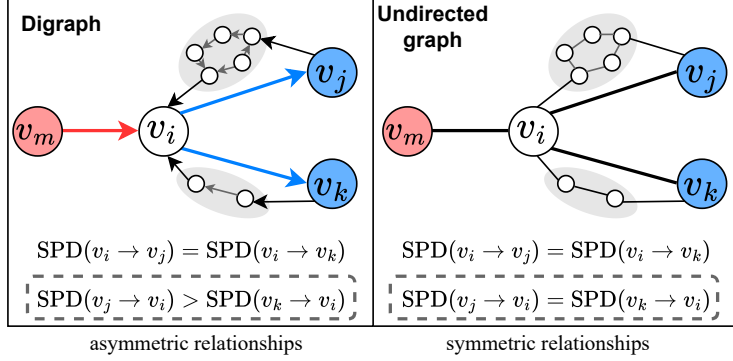


Figure 1: A digraph and its undirected counterpart. Blue arrows indicate unidirectional paths, together with longer paths in the gray area, forming commute closed loops between the central node v_i and its outgoing neighbors v_j and v_k . In the undirected graph, shortest path distances (SPD) between nodes are symmetric. However, in the digraph, the fact that unidirectional SPDs are equal does not imply that mutual SPDs will also be equal. For instance, while the SPD from v_i to v_j and v_k is identical, the reverse SPD from v_j and v_k back to v_i do not necessarily match this distance.

are both immediate outgoing neighbors of v_i , the strength of their relationships with the central node differs significantly. Existing methods (Rossi et al., 2023; Tong et al., 2020b; Zhang et al., 2021), by focusing solely on unidirectional shortest paths (blue and red arrows), fail to capture the asymmetry phenomenon, which conveys valuable information of node relationships. Take social networks as an example: an ordinary user can directly follow a celebrity, yielding a short path to the celebrity, yet the reverse path from the celebrity to the follower might be much longer. Considering only the short path from the follower to celebrity could falsely suggest a level of closeness that does not exist. In contrast, accounting for the mutual paths between users yields a more precise and robust measure of their relationship, with stronger mutual interactions implying stronger connections.

To capture the mutual path interactions in GNNs, we adapt the concept of commute time, the expected number of steps to traverse from a source node to a target and back, from the Markov chain theory to the domain of graph learning. To this end, we first generalize the graph Laplacian to the digraph by defining the divergence of the gradient on the digraph. Utilizing this digraph-specific Laplacian, we develop an efficient method to compute commute time, ensuring sparsity and computational feasibility. Then we incorporate the commute-time-based proximity measure into the message passing process by assigning aggregation weights to neighbors. The intuition behind is that the immediate and unidirectional neighboring relationships do not necessarily imply strong similarity, but the mutual proximity is a more reliable indicator of relationship closeness. Our experimental results demonstrate the effectiveness of CGNN.

2 Related Work

2.1 Digraph Laplacian

While the Laplacian for undirected graphs has been extensively studied, the area of Laplace operator digraphs remains underexplored. Chung (2005) pioneers this area by defining a normalized Laplace operator specifically for strongly connected directed graphs with nonnegative weights. This operator is expressed as $\mathbf{I} - \frac{\pi^{1/2} \mathbf{P} \pi^{-1/2} + \pi^{-1/2} \mathbf{P}^* \pi^{1/2}}{2}$. Key to this formulation is the use of the transition probability operator \mathbf{P} and the Perron vector π , with the operator being self-adjoint. Building on the undirected graph Laplacian, Singh et al. (2016) adapt this concept to accommodate the directed structure, focusing particularly on the in-degree matrix. They define the directed graph Laplacian as $\mathbf{D}_{\text{in}} - \mathbf{A}$, where $\mathbf{D}_{\text{in}} = \text{diag} \left(\{d_i^{\text{in}}\}_{i=1}^N \right)$ represents the in-degree matrix. Li & Zhang (2012) uses stationary probabilities of the Markov chain governing random walks on digraphs to define the Laplacian as $\pi^{\frac{1}{2}} (\mathbf{I} - \mathbf{P}) \pi^{-\frac{1}{2}}$, which underscores the importance of random walks and their stationary distributions in understanding digraph dynamics. Hermitian Laplacian Furutani et al. (2020) consider the edge directionality and node connectivity separately, and encode the edge direction into the argument in the complex plane. Diverging from existing Laplacians, our proposed DiLap

$\Pi(\mathbf{D}^{-1} - \mathbf{P})$ is grounded in graph signal processing principles, conceptualized as the divergence of a signal’s gradient on the digraph. It encompasses the degree matrix \mathbf{D} to preserve local connectivity, the transition matrix \mathbf{P} to maintain the graph’s directed structure, and the diagonalized Perron vector Π , capturing critical global graph attributes such as node structural importance, global connectivity, and expected reachability (Chung, 1997).

2.2 Digraph Neural Networks

To effectively capture the directed structure with GNNs, spectral-based methods (Zhang et al., 2021; Tong et al., 2020a,b) have been proposed to preserve the underlying spectral properties of the digraph by performing spectral analysis based on the digraph Laplacian proposed by (Chung, 2005). MagNet (Zhang et al., 2021) utilizes magnetic Laplacian to derive a complex-valued Hermitian matrix to encode the asymmetric nature of digraphs. Spatial GNNs also offer a natural approach to capturing directed structures. For instance, GraphSAGE (Hamilton et al., 2017) allows for controlling the direction of information flow by considering in-neighbors or out-neighbors separately. DirGNN (Rossi et al., 2023) further extends this framework by segregating neighbor aggregation according to edge directions, offering a more refined method to handle the directed nature of graphs.

3 Random Walk Distance and GNNs

We start by establishing the notations. We then show that message passing based GNNs naturally capture the concept of hitting time during information propagation across the graph, due to the unidirectional nature of the neighborhood aggregation. Subsequently, we argue for the significance of commute time, highlighting it as a more compact measure of mutual node-wise interactions in random walks.

Notations Consider $G = (V, E, \mathbf{X})$ as an unweighted digraph comprising N nodes, where $V = \{v_i\}_{i=1}^N$ is the node set, $E \subseteq (V \times V)$ is the edge set, $\mathbf{X} \in \mathbb{R}^{N \times d}$ is the node feature matrix. $Y = \{y_1, \dots, y_N\}$ is the set of labels for V . Let $\mathbf{A} \in \mathbb{R}^{N \times N}$ be the adjacency matrix and $\mathbf{D} = \text{diag}(d_1, \dots, d_N) \in \mathbb{R}^{N \times N}$ be the degree matrix of \mathbf{A} , where $d_i = \sum_{v_j \in V} \mathbf{A}_{ij}$ is the out-degree of v_i . Let $\tilde{\mathbf{A}} = \mathbf{A} + \mathbf{I}$ and $\tilde{\mathbf{D}} = \mathbf{D} + \mathbf{I}$ denote the adjacency and degree matrix with self-loops, respectively. The transition probability matrix of the Markov chain associated with random walks on G is defined as $\mathbf{P} = \mathbf{D}^{-1} \mathbf{A}$, where $\mathbf{P}_{ij} = \mathbf{A}_{ij}/\deg(v_i)$ is the probability of a 1-step random walk starting from v_i to v_j . Graph Laplacian formalized as $\mathbf{L} = \mathbf{D} - \mathbf{A}$ is defined on the undirected graph whose adjacency matrix is symmetric. The symmetrically normalized Laplacian with self-loops (Wu et al., 2019) is defined as $\hat{\mathbf{L}} = \tilde{\mathbf{D}}^{-\frac{1}{2}} \tilde{\mathbf{L}} \tilde{\mathbf{D}}^{-\frac{1}{2}}$, where $\tilde{\mathbf{L}} = \tilde{\mathbf{D}} - \tilde{\mathbf{A}}$.

Digraph Neural Networks DirGNN (Rossi et al., 2023) is a general framework that generalizes the message passing paradigm to digraphs by adapting to the directionality of edges. It involves separate aggregation processes for incoming and outgoing neighbors of each node as follows:

$$\begin{aligned} m_{i,\text{in}}^{(\ell)} &= \text{Agg}_{\text{in}}^{(\ell)} \left(\left\{ h_j^{(\ell-1)} : v_j \in \mathcal{N}_i^{\text{in}} \right\} \right) \\ m_{i,\text{out}}^{(\ell)} &= \text{Agg}_{\text{out}}^{(\ell)} \left(\left\{ h_j^{(\ell-1)} : v_j \in \mathcal{N}_i^{\text{out}} \right\} \right) \\ h_i^{(\ell)} &= \text{Comb}^{(\ell)} \left(h_i^{(\ell-1)}, m_{i,\text{in}}^{(\ell)}, m_{i,\text{out}}^{(\ell)} \right), \end{aligned} \quad (1)$$

where $\mathcal{N}_i^{\text{in}}$ and $\mathcal{N}_i^{\text{out}}$ are respectively incoming and outgoing neighbors of v_i . $\text{Agg}_{\text{in}}^{(\ell)}(\cdot)$ and $\text{Agg}_{\text{out}}^{(\ell)}(\cdot)$ are specialized aggregation functions of $\mathcal{N}_i^{\text{in}}$ and $\mathcal{N}_i^{\text{out}}$ at layer ℓ , used to encode the directional characteristics of the edges connected to v_i .

3.1 Can GNNs Capture Random Walk Distance?

In the context of random walks on a digraph, hitting time and commute time, collectively referred to as random walk distances, serve as key metrics for assessing node connectivity and interaction strength. Hitting time $h(v_i, v_j)$ is the expected number of steps a random walk takes to reach a specific target node v_j for the first time, starting from a given source node v_i . Commute time $c(v_i, v_j)$ is the expected number of steps required for a random walk to start at v_i , reach v_j , and come back. A

high hitting (commute) time indicates difficulty in achieving unidirectional (mutual) visits to each other in a random walk. As illustrated in the digraph of Fig. 1, commute time $c(v_i, v_j) > c(v_i, v_k)$, while the hitting time $h(v_m, v_i) = h(v_i, v_j) = h(v_i, v_k)$.

Motivation Given these definitions, two questions arise: How crucial is it to retain these measures in graph learning? Also, are message-passing GNNs capable of preserving these characteristics? Firstly, both hitting time and commute time are critical in understanding the structural dynamics of graphs. Hitting time, analogous to the shortest path, measures the cost of reaching one node from another, reflecting the directed influence or connectivity. Commute time, encompassing the round-trip journey, offers insights into the mutual relationships between nodes, which is especially evident in social networks, as illustrated by celebrity-follower relationships. Secondly, message-passing GNNs are somewhat effective in capturing hitting time, as they propagate information across the graph in a manner similar to a random walk, where quickly reached nodes are preferentially aggregated, and the influence of nodes exponentially diminishes with increasing distance (Topping et al., 2022). However, GNNs face challenges in preserving commute time due to their requirement for comprehending mutual path relations, which are inherently asymmetric and often involve longer-range interactions especially in digraphs, which are not naturally captured in the basic message-passing framework.

Taking the digraph in Fig. 1 as an example, a 1-layer DirGNN defined in Eq. (1) can encode v_m , v_j and v_k into the representation of v_i , while also capturing the directionality of edges from these neighbors by using distinct aggregation functions for incoming and outgoing neighbors. It shows that DirGNN can capture the hitting time, as neighbors with lower hitting times, $h(v_i, v_k)$, $h(v_i, v_k)$ and $h(v_m, v_i)$, are aggregated preferentially. However, DirGNN inherently focuses on unidirectional interactions and overlooks mutual path dependencies. Notably, a 1-layer DirGNN is insufficient for capturing the asymmetric interactions indicated by the paths from v_j and v_k returning to the central node v_i (gray areas). One potential approach to address this limitation is to stack additional message passing layers to encompass the entire commute path between nodes, thereby capturing mutual path interactions. Nevertheless, this strategy is non-trivial because the commute paths vary considerably across different node pairs, complicating the determination of an appropriate number of layers. Additionally, stacking multiple layers to cover these paths can introduce irrelevant non-local information and lead to oversmoothing.

Goal We expect to directly encode node-wise commute time into the node representations to accurately reflect the true interaction strength between *adjacent* nodes during neighbor aggregation, accounting for both forward and backward paths. For instance, even though $h(v_i, v_j) = h(v_i, v_k)$, a shorter commute time $c(v_i, v_k) < c(v_i, v_j)$ suggests a stronger interaction from v_k to v_i compared to v_j to v_i . Consequently, the contribution of neighbor v_k to the representation of v_i should be greater than that of v_j .

3.2 Commute Time Computation

Based on the standard Markov chain theory, a useful tool to study random walk distances is the fundamental matrix (Aldous & Fill, 2002). We first establish the following assumptions required to support the theorem.

Assumption 3.1. *The digraph G is irreducible and aperiodic.*

These two properties pertain to the Markov chain’s stationary probability distribution π (i.e., Perron vector) corresponding to the given graph. Irreducibility ensures that it is possible to reach any node (state) from any other node, preventing π from converging to 0. Aperiodicity ensures that the Markov chain does not get trapped in cycles of a fixed length, thus guaranteeing the existence of a unique π . Existence and uniqueness of π facilitate deterministic analysis and computation. For a more intuitive understanding of the assumptions, we give the sufficient conditions of digraph under the irreducibility and aperiodicity assumptions.

Proposition 1. *A strongly connected digraph, in which a directed path exists between every pair of vertices, is irreducible. A digraph with self-loops in each node is aperiodic.*

Given the above assumption, the fundamental matrix \mathbf{Z} is defined as the sum of an infinite matrix series:

$$\mathbf{Z} = \sum_{t=0}^{\infty} (\mathbf{P}^t - \mathbf{J}\mathbf{\Pi}) = \sum_{t=0}^{\infty} (\mathbf{P}^t - e\pi^{\top}), \quad (2)$$

where e is the all-one column vector, then we have $\mathbf{J} = e \cdot e^{\top}$ is the all-one matrix, and $\mathbf{\Pi} = \text{diag}(\pi)$ is the diagonal matrix of π .

Theorem 3.2. (Li & Zhang, 2012) *Given Assumption 3.1, the fundamental matrix \mathbf{Z} defined in Eq. (2) converges to:*

$$\mathbf{Z} = (\mathbf{I} - \mathbf{P} + \mathbf{J}\mathbf{\Pi})^{-1} - \mathbf{J}\mathbf{\Pi}, \quad (3)$$

where \mathbf{I} is an identity matrix.

The hitting time and commute time on G can then be expressed as \mathbf{Z} (Aldous & Fill, 2002) as follows:

$$h(v_i, v_j) = \frac{\mathbf{Z}_{jj} - \mathbf{Z}_{ij}}{\pi_j}, \quad c(v_i, v_j) = h(v_i, v_j) + h(v_j, v_i). \quad (4)$$

However, directly calculating the complete fundamental matrix \mathbf{Z} and the commute times for all node pairs is computationally expensive and yields a dense matrix. Moreover, integrating the random walk distances computation, defined in Eq. (3) and Eq. (4), into the message passing framework is non-trivial, which concerns the scalability of the model.

4 Commute Graph Neural Networks

In this section, we present **Commute Graph Neural Networks** (CGNN) to encode the commute time information into message passing. We first establish the relationship between random walk distances and the digraph Laplacian.

4.1 Digraph Laplacian (DiLap)

Contrary to the traditional graph Laplacian, typically defined as a symmetric positive semi-definite matrix derived from the symmetric adjacency matrix, our proposed DiLap is built upon the transition matrix to preserve the directed structure. Specifically, the classical graph Laplacian $\mathbf{L} = \mathbf{D} - \mathbf{A}$ is interpreted as the divergence of the gradient of a signal on an undirected graph (Shuman et al., 2013; Hamilton, 2020): given a graph signal $s \in \mathbb{R}^N$, $(\mathbf{L}s)_i = \sum_{j \in \mathcal{N}_i} \mathbf{A}_{ij}(s_i - s_j)$. Intuitively, graph Laplacian corresponds to the difference operator on the signal s , and acts as a node-wise measure of local smoothness. In line with this conceptual foundation, we generalize the graph Laplacian to digraphs by defining DiLap \mathbf{T} :

$$(\mathbf{T}s)_i = \sum_{v_j \in \mathcal{N}_i^{\text{out}}} \mathbf{P}_{ij}(s_i - s_j) = ((\mathbf{D}^{-1} - \mathbf{P})s)_i, \quad \text{we have } \mathbf{T} = \mathbf{D}^{-1} - \mathbf{P}, \quad (5)$$

where $\mathcal{N}_i^{\text{out}}$ is the set of v_i 's out-neighbors, and $\mathbf{P}_{ij} = \frac{1}{d_i^{\text{out}}}$ with d_i^{out} being the out-degree of v_i . The detailed derivation of \mathbf{T} is included in Appendix A.1. Eq. (5) illustrates that DiLap \mathbf{T} acts as the divergence of the gradient of a given signal on a digraph, and can be used to measure the local smoothness in a digraph.

Considering the Laplacian operator's function in measuring the smoothness of a signal across the entire graph, it is crucial to assign greater weights to nodes of higher structural importance. It is because the smoothness at nodes central to the graph structure should have a more pronounced impact on the global smoothness measurement. Thus, we further define the Weighted DiLap \mathcal{T} :

$$(\mathcal{T}s)_i = \sum_{v_j \in \mathcal{N}_i^{\text{out}}} \pi_i \mathbf{P}_{ij}(s_i - s_j) = (\mathbf{\Pi}(\mathbf{D}^{-1} - \mathbf{P})s)_i, \quad \text{we have } \mathcal{T} = \mathbf{\Pi}(\mathbf{D}^{-1} - \mathbf{P}). \quad (6)$$

Here we utilize the i -th element of the Perron vector π to quantify the structural importance of v_i , reflecting its eigenvector centrality. This is based on the principle that a node's reachability is directly proportional to its corresponding value in the Perron vector (Xu et al., 2018). Therefore, π effectively indicates the centrality and influence over the long term in the graph. Perron-Frobenius Theorem (Horn & Johnson, 2012) establishes that π satisfies $\sum_i \pi(i) = 1$, is strictly positive, and converges to the left eigenvector of the dominant eigenvalue of \mathbf{P} .

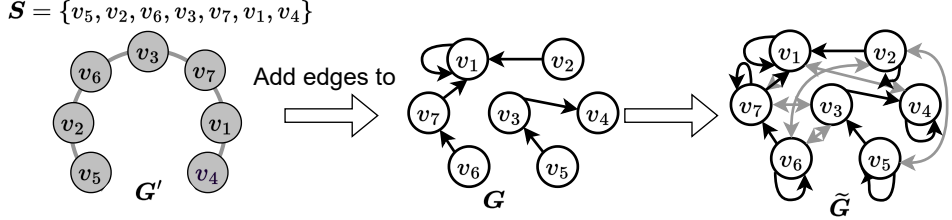


Figure 2: The sorted node indices in S are connected one by one with undirected edges to construct G' , then adding all edges from G' to G to generate \tilde{G} .

4.2 Similarity-based Graph Rewiring

Both the fundamental matrix defined in Eq. (3) and Weighted DiLap requires Assumption 3.1 to ensure the existence and uniqueness of the Perron vector π , conditions that are not universally met in general graphs. To fulfill the irreducibility and aperiodicity assumptions, Tong et al. (2020a) introduce a teleporting probability uniformly distributed across all nodes. This method, inspired by PageRank (Page et al., 1999), amends the transition matrix to $\mathbf{P}_{pr} = \gamma \mathbf{P} + (1 - \gamma) \frac{ee^\top}{N}$, where $\gamma \in (0, 1)$. \mathbf{P}_{pr} allows for the possibility that a random walker may choose a non-neighbor node for the next step with a probability of $\frac{1-\gamma}{N}$. This adjustment ensures that \mathbf{P}_{pr} is irreducible and aperiodic, so it has a unique π . However, this approach leads to a complete graph represented by a dense matrix \mathbf{P}_{pr} , posing significant challenges for subsequent computational processes.

Rather than employing \mathbf{P}_{pr} as the transition matrix, we introduce a graph rewiring method based on feature similarity to make a given graph irreducible, while maintaining the sparsity. As outlined in Proposition 1, to transform the digraph into a strongly connected structure, it is essential that each node possesses a directed path to every other node. To this end, we initially construct a simple and irreducible graph G' with all N nodes, then add all edges from G' to the original digraph G , thereby ensuring G 's irreducibility. The construction of G' begins with the calculation of the mean of node features as the anchor vector \mathbf{a} . Then we determine the similarity between each node and the anchor, sort the similarity values, and return the sorted node indices, denoted as $S \in \mathbb{R}^N$:

$$\mathbf{a} = \frac{\sum_i \mathbf{X}_i}{N}, \quad s_i = \cos(\mathbf{a}, \mathbf{X}_i), \quad S = \text{argsort}(\{s_i\}_{i=1}^N) \quad (7)$$

where $\cos(\mathbf{a}, \mathbf{X}_i)$ is the cosine similarity between node features of v_i and \mathbf{a} , and $\text{argsort}(\cdot)$ yields the indices of nodes that sort similarity values $\{s_i\}_{i=1}^N$. We then connect the nodes one by one with undirected (bidirectional) edges following the order in S to construct G' , as shown in Fig. 2. Given that G' is strongly connected, adding all its edges into G results in a strongly connected digraph \tilde{G} , which is irreducible. To achieve aperiodicity, self-loops are further added to \tilde{G} .

This rewiring approach satisfies Assumption 3.1 and maintains graph sparsity. Additionally, adding edges between nodes with similar features only minimally alters the overall semantics of the original graph. Based on \tilde{G} and its corresponding $\tilde{\mathbf{P}}$ and $\tilde{\mathbf{\Pi}}$, we have the deterministic Weighted DiLap $\tilde{\mathcal{T}}$.

4.3 From DiLap to Commute Time

Given the Weighted DiLap $\tilde{\mathcal{T}}$, we can unify the commute time information into the message passing by building the connection between $\tilde{\mathcal{T}}$ and the fundamental matrix \mathbf{Z} :

Lemma 4.1. *Given a rewired graph \tilde{G} , the Weighted DiLap is defined as $\tilde{\mathcal{T}} = \tilde{\mathbf{\Pi}}(\tilde{\mathbf{D}}^{-1} - \tilde{\mathbf{P}})$. Then the fundamental matrix \mathbf{Z} of \tilde{G} can be solved by:*

$$\mathbf{Z} = \tilde{\mathbf{\Pi}}^{-\frac{1}{2}} \mathcal{R}^\dagger \tilde{\mathbf{\Pi}}^{\frac{1}{2}}, \quad (8)$$

where $\mathcal{R} = \tilde{\mathbf{\Pi}}^{-\frac{1}{2}} \tilde{\mathcal{T}} \tilde{\mathbf{\Pi}}^{-\frac{1}{2}} - \tilde{\mathbf{D}}^{-1} + \mathbf{I}$ and the superscript \dagger means Moore–Penrose pseudoinverse of the matrix.

The proof is given in Appendix A.2. Leveraging Lemma 4.1, we can further compute the hitting times and commute times in terms of $\tilde{\mathcal{T}}$ with the following theorem.

Theorem 4.2. Given \tilde{G} , the hitting time and commute time from v_i to v_j on \tilde{G} can be computed as follows:

$$h(v_i, v_j) = \frac{\mathcal{R}_{jj}^\dagger}{\pi_j} - \frac{\mathcal{R}_{ij}^\dagger}{\sqrt{\pi_i \pi_j}},$$

$$c(v_i, v_j) = h(v_i, v_j) + h(v_j, v_i) = \frac{\mathcal{R}_{jj}^\dagger}{\pi_j} + \frac{\mathcal{R}_{ii}^\dagger}{\pi_i} - \frac{\mathcal{R}_{ij}^\dagger}{\sqrt{\pi_i \pi_j}} - \frac{\mathcal{R}_{ji}^\dagger}{\sqrt{\pi_i \pi_j}}. \quad (9)$$

For a detailed proof of this theorem, refer to Theorem 3 in (Li & Zhang, 2012), where the corresponding term should be replaced with \mathcal{R} . Then we can derive the matrix forms of the hitting time \mathcal{H} and commute time \mathcal{C} as per Eq. (9):

$$\mathcal{H} = (e \otimes \pi^{-1})(\mathcal{R}^\dagger \odot \mathbf{I}) - \mathcal{R}^\dagger \odot (\pi^{-\frac{1}{2}} \otimes \pi^{-\frac{1}{2}}), \quad \mathcal{C} = \mathcal{H} + \mathcal{H}^\top \quad (10)$$

where \odot denotes Hadamard product, and \otimes is outer product. \mathcal{H}_{ij} and \mathcal{C}_{ij} correspond to the hitting and commute time from v_i to v_j respectively. The computation of commute times via DiLap, in contrast to the method delineated in Theorem 3.2, is primarily motivated by efficiency concerns. Specifically, Eq. (3) necessitates the inversion of a dense matrix with complexity $\mathcal{O}(N^3)$, whereas our DiLap-based method hinges on computing the pseudoinverse of a sparse matrix \mathcal{R} . The pseudoinverse of \mathcal{R} can be efficiently determined using SVD. Given the sparse nature of \mathcal{R} , we can employ well-established techniques such as the randomized truncated SVD algorithm (Halko et al., 2011; Cai et al., 2023), which takes advantage of sparsity, to reduce the time complexity to $\mathcal{O}(q|E|)$, where $|E|$ denotes the number of edges reflecting the sparsity (See Appendix A.3). Next, we present Commute Graph Neural Networks (CGNN) based on \mathcal{C} .

4.4 CGNN

$\mathcal{C} \in \mathbb{R}^{N \times N}$ quantifies the strength of mutual relations between node pairs in the random walk context. Notably, smaller values in \mathcal{C} correspond to stronger mutual reachability, indicating stronger relations between node pairs. Thus, \mathcal{C} is a positive symmetric matrix, and the commute-time-based node proximity matrix can be expressed as $\tilde{\mathcal{C}} = \exp(-\mathcal{C})$. Since the directed adjacency matrix \mathbf{A} represents the outgoing edges of each node, \mathbf{A}^\top therefore accounts for all incoming edges. Then we have $\tilde{\mathcal{C}}^{\text{out}} = \mathbf{A} \odot \tilde{\mathcal{C}}$ and $\tilde{\mathcal{C}}^{\text{in}} = \mathbf{A}^\top \odot \tilde{\mathcal{C}}$ represent the proximity between adjacent nodes under outgoing and incoming edges, respectively. We further perform row-wise max-normalization on $\tilde{\mathcal{C}}^{\text{out}}$ and $\tilde{\mathcal{C}}^{\text{in}}$ to rescale the maximum value in each row to 1. Given the original graph G as input, we define the ℓ -th layer of CGNN as:

$$m_{i,\text{in}}^{(\ell)} = \text{Agg}_{\text{in}}^{(\ell)} \left(\left\{ \tilde{\mathcal{C}}_{ij}^{\text{in}} \cdot h_j^{(\ell-1)} : v_j \in \mathcal{N}_i^{\text{in}} \right\} \right)$$

$$m_{i,\text{out}}^{(\ell)} = \text{Agg}_{\text{out}}^{(\ell)} \left(\left\{ \tilde{\mathcal{C}}_{ij}^{\text{out}} \cdot h_j^{(\ell-1)} : v_j \in \mathcal{N}_i^{\text{out}} \right\} \right)$$

$$h_i^{(\ell)} = \text{Comb}^{(\ell)} \left(h_i^{(\ell-1)}, m_{i,\text{in}}^{(\ell)}, m_{i,\text{out}}^{(\ell)} \right), \quad (11)$$

where $\text{Agg}_{\text{in}}^{(\ell)}(\cdot)$ and $\text{Agg}_{\text{out}}^{(\ell)}(\cdot)$ are mean aggregation functions with different feature transformation weights, and $\text{Comb}^{(\ell)}(\cdot)$ is a mean operator. Within each layer, the influence of v_j on the central node v_i is modulated by the commute-time-based proximity $\tilde{\mathcal{C}}$ based on the edge directionality. We present the pseudocode and complexity of CGNN in Algorithm 1.

5 Experiments

We conduct node classification experiments on five digraph datasets. Experimental details and data statistics are provided in Appendix C.1 and Appendix C.2. We provide a performance comparison with 12 baselines including 1) General GNNs: GCN (Kipf & Welling, 2017), GAT (Veličković et al., 2018), and GraphSAGE (Hamilton et al., 2017); 2) Non-local GNNs: APPNP (Klicpera et al., 2019), MixHop (Abu-El-Haija et al., 2019), GPRGNN (Chien et al., 2021), and GCNII (Ming Chen et al., 2020); 3) Digraph NNs: DGCN (Tong et al., 2020b), DiGCN (Tong et al., 2020a), MagNet (Zhang et al., 2021), DiGCL (Tong et al., 2021), and DirGNN (Rossi et al., 2023). For all baselines, we apply both the symmetrized and asymmetric adjacency matrix for experiments. The results reported are the better of the two results.

Table 1: Node classification results. Accuracy (%) with standard deviation for 10 runs. We highlight/underline the best/second best method. For general GNN and non-local GNN baselines, we conduct experiments on both symmetrized versions and their directed counterparts, reporting better results from these two settings.

Method	Squirrel	Chameleon	Citeseer	CoraML	AM-Photo
GCN	52.43 \pm 2.01	67.96 \pm 1.82	66.03 \pm 1.88	70.92 \pm 0.39	88.52 \pm 0.47
GAT	40.72 \pm 1.55	60.69 \pm 1.95	65.58 \pm 1.39	72.22 \pm 0.57	88.36 \pm 1.25
GraphSAGE	41.61 \pm 0.74	62.01 \pm 1.06	66.81 \pm 1.38	74.16 \pm 1.55	89.71 \pm 0.57
APPNP	51.91 \pm 0.56	45.37 \pm 1.62	66.90 \pm 1.82	70.31 \pm 0.67	87.43 \pm 0.98
MixHop	43.80 \pm 1.48	60.50 \pm 2.53	56.09 \pm 2.08	65.89 \pm 1.50	87.17 \pm 1.34
GPRGNN	50.56 \pm 1.51	66.31 \pm 2.05	61.74 \pm 1.87	73.31 \pm 1.37	90.23 \pm 0.34
GCNII	38.47 \pm 1.58	63.86 \pm 3.04	58.32 \pm 1.93	64.84 \pm 0.71	83.40 \pm 0.79
DGCN	37.16 \pm 1.72	50.77 \pm 3.31	66.37 \pm 1.93	75.02 \pm 0.50	87.74 \pm 1.02
DiGCN	33.44 \pm 2.07	50.37 \pm 4.31	64.99 \pm 1.72	77.03 \pm 0.70	88.66 \pm 0.51
MagNet	39.01 \pm 1.93	58.22 \pm 2.87	65.04 \pm 0.47	76.32 \pm 0.10	86.80 \pm 0.65
DiGCL	35.82 \pm 1.73	56.45 \pm 2.77	67.42 \pm 0.14	77.53 \pm 0.14	89.41 \pm 0.11
DirGNN	75.19 \pm 1.26	79.11 \pm 2.28	66.57 \pm 0.74	75.33 \pm 0.32	88.09 \pm 0.46
CGNN	77.20\pm2.42	79.54\pm1.82	70.27\pm0.66	77.02 \pm 0.67	90.41\pm0.32

5.1 Overall Results

Table 1 reports the node classification results across five digraph datasets. Our method CGNN achieves new state-of-the-art results on 4 out of 5 datasets, and comparable results on the remaining one, validating the superiority of CGNN. We provide more observations as follows. Firstly, while non-local GNNs have the potential to cover the commute paths between adjacent nodes by stacking multiple layers, they do not consistently outperform general, shallow GNN models. It suggests that coarsely aggregating all nodes in commute paths is ineffective. The reason is that deeper models may aggregate excessive irrelevant information for the central node. Our goal is to encode mutual relationships between adjacent nodes by considering their commute times. Aggregating all nodes along the entire path introduces excessive information about other nodes unrelated to the direct relationship between the target nodes. Secondly, GNNs tailored for digraphs do not seem to bring substantial gains. Our results show that with careful hyper-parameter tuning, general GNNs can achieve results comparable to, or even better than, those tailored for digraphs, as evidenced in the Squirrel, Chameleon, and AM-Photo datasets. Thirdly, CGNN achieves state-of-the-art results on both homophilic and heterophilic digraph benchmarks. Notably, DirGNN also performs comparably on heterophilic graphs (Squirrel and Chameleon), supporting the findings of Rossi et al. (2023) that distinguishing edge directionality during message passing enables the central node to adaptively balance information flows from both heterophilic and homophilic neighbors, effectively mitigating the impact of heterophily. Moreover, CGNN, an enhanced version of DirGNN, further improves performance on these graphs by effectively incorporating commute times to refine the strength of relationships between nodes, enhancing model robustness under heterophily.

To illustrate this, we further examine the relations between commute-time-based proximity and label similarity along edges. As shown in Eq. (11), we use commute-time-based proximity $\tilde{\mathcal{C}}$ to weigh the neighbors during neighbor aggregation. Then we define a label similarity matrix \mathcal{M} where $\mathcal{M}_{ij} = 1$ if $v_j \in \mathcal{N}_i$ and $y_i = y_j$; otherwise $\mathcal{M}_{ij} = 0$. Essentially, \mathcal{M} extracts the edges connecting nodes with the same classes from the adjacency matrix \mathbf{A} . Thus a higher value of $\|\mathcal{M} - (\mathbf{A} + \mathbf{A}^\top)\|_2^2$ indicates a more pronounced negative impact of heterophily on the model’s performance. On the other hand, we compute $\|\mathcal{M} - (\tilde{\mathcal{C}}^{\text{in}} + \tilde{\mathcal{C}}^{\text{out}})\|_2^2$ to evaluate the efficacy of $\tilde{\mathcal{C}}$ in filtering heterophilic information. The closer $(\tilde{\mathcal{C}}^{\text{in}} + \tilde{\mathcal{C}}^{\text{out}})$ is to \mathcal{M} , the more effectively it aids the model in discarding irrelevant heterophilic information. Table 2 visually demonstrates these relationships. We observe that in heterophilic datasets, the commute-time-based proximity matrix $(\tilde{\mathcal{C}}^{\text{in}} + \tilde{\mathcal{C}}^{\text{out}})$, aligns more closely with the label similarity matrix \mathcal{M} than $(\mathbf{A} + \mathbf{A}^\top)$. It indicates that $\tilde{\mathcal{C}}$ effectively filters out irrelevant information during message passing by appropriately weighting neighbors, which explains the exceptional performance of CGNN on heterophilic datasets.

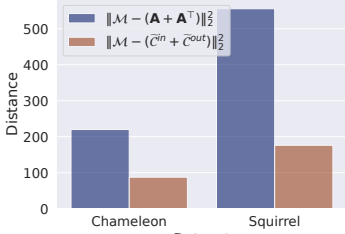


Table 2: The distance between \mathcal{M} and \mathbf{A} , and between \mathcal{M} and $\tilde{\mathcal{C}}$.

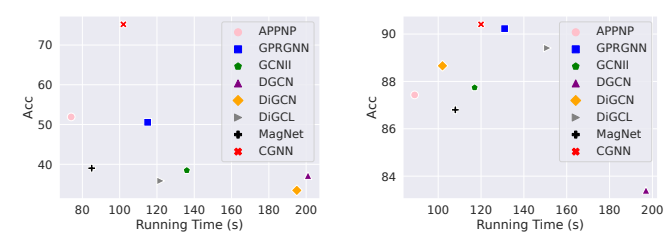


Figure 3: Accuracy vs. running time on Squirrel and AM-Photo.

5.2 Efficiency Comparsion

Fig. 3 compares the accuracy of CGNN and other baseline models with their running times. Despite the additional computational load of calculating commute-time-based proximity, the results show that CGNN provides the best trade-off between effectiveness and efficiency. In particular, on the Squirrel dataset, CGNN has the third-fastest calculation speed while yielding accuracy nearly double that of all other methods. On AM-Photo, CGNN achieves the highest accuracy while maintaining moderate efficiency.

5.3 Component Analysis

Comparison between graph rewiring and PPR. In Section 4.2, we construct a rewired graph \tilde{G} based on feature similarity to guarantee the irreducibility and aperiodicity. On the other hand, In contrast, the classic PageRank transition matrix, defined as $\mathbf{P}_{pr} = \gamma \mathbf{P} + (1 - \gamma) \frac{ee^\top}{N}$, achieves a similar objective but results in a completely connected graph G_{pr} . However, this approach tends to overlook the sparse structure of the original graph, which may alter the semantic information in the graph. Additionally, computing commute times using a dense transition matrix incurs a high computational cost. To validate the effectiveness of the rewiring approach over the PPR method, we conduct an experiment where \tilde{G} is replaced with G_{pr} in the computation of commute-time-based proximity. We denote this variant as ‘CGNN_{ppr}’ and the results of accuracy and efficiency are reported in Table 3. The findings reveal that the PPR approach is suboptimal in terms of both accuracy and efficiency, thereby underscoring the effectiveness of our rewiring-based approach.

Table 3: Accuracy and running time (s) of CGNN and CGNN_{ppr}.

Method	Squirrel		Chameleon		Citeseer		CoraML		AM-Photo	
	Acc.	Time	Acc.	Time	Acc.	Time	Acc.	Time	Acc.	Time
CGNN	77.20	102.93	79.54	112.24	80.27	92.26	77.02	127.15	90.41	121.80
CGNN _{ppr}	68.37	257.84	71.69	253.05	78.59	137.82	76.23	192.09	88.52	203.04

Directed vs. Undirected. To validate the critical role of directed structures in our model, we transform all directed edges into undirected ones by adding their reverse counterparts. This process results in a symmetric adjacency matrix, denoted as \mathbf{A}_{sym} . Subsequently, the commute time is calculated based on the transition matrix derived from \mathbf{A}_{sym} . We refer this variant as ‘CGNN_{sym}’. Fig. 4 shows the accuracy of CGNN and CGNN_{sym} on three datasets. We find that edge direction can significantly influence the prediction accuracy for our model.

Figure 4: Impact of directed structure.

	Squirrel	CoraML	AM-Photo
CGNN	77.20	77.02	90.41
CGNN _{sym}	71.31	70.25	88.42

6 Conclusion

In this work, we introduce the Commute Graph Neural Network (CGNN) to integrate commute time into GNNs for digraphs. To this end, we propose DiLap, a new Laplacian formulation for digraphs, along with a rapid computational method for determining commute times. By integrating commute times into GNN message passing through neighbor weighting, CGNN effectively leverages

the path asymmetry in digraphs, thus improving node representation learning. Our comprehensive experiments demonstrate the superior performance of CGNN over existing methods.

References

Abu-El-Haija, S., Perozzi, B., Kapoor, A., Alipourfard, N., Lerman, K., Harutyunyan, H., Ver Steeg, G., and Galstyan, A. Mixhop: Higher-order graph convolutional architectures via sparsified neighborhood mixing. In *international conference on machine learning*, pp. 21–29. PMLR, 2019.

Aldous, D. and Fill, J. Reversible markov chains and random walks on graphs, 2002.

Bojchevski, A. and Günnemann, S. Deep gaussian embedding of attributed graphs: Unsupervised inductive learning via ranking. *arXiv preprint arXiv:1707.03815*, 2017.

Cai, X., Huang, C., Xia, L., and Ren, X. Lightgcl: Simple yet effective graph contrastive learning for recommendation. *arXiv preprint arXiv:2302.08191*, 2023.

Chien, E., Peng, J., Li, P., and Milenkovic, O. Adaptive universal generalized pagerank graph neural network. In *International Conference on Learning Representations*, 2021. URL <https://openreview.net/forum?id=n6j17fLxrP>.

Chung, F. Laplacians and the cheeger inequality for directed graphs. *Annals of Combinatorics*, 9(1): 1–19, 2005.

Chung, F. R. *Spectral graph theory*, volume 92. American Mathematical Soc., 1997.

Cross, R., Borgatti, S. P., and Parker, A. Beyond answers: Dimensions of the advice network. *Social networks*, 23(3):215–235, 2001.

Furutani, S., Shibahara, T., Akiyama, M., Hato, K., and Aida, M. Graph signal processing for directed graphs based on the hermitian laplacian. In *Machine Learning and Knowledge Discovery in Databases: European Conference, ECML PKDD 2019, Würzburg, Germany, September 16–20, 2019, Proceedings, Part I*, pp. 447–463. Springer, 2020.

Geisler, S., Li, Y., Mankowitz, D. J., Cemgil, A. T., Günnemann, S., and Paduraru, C. Transformers meet directed graphs. In *International Conference on Machine Learning*, pp. 11144–11172. PMLR, 2023.

Halko, N., Martinsson, P.-G., and Tropp, J. A. Finding structure with randomness: Probabilistic algorithms for constructing approximate matrix decompositions. *SIAM review*, 53(2):217–288, 2011.

Hamilton, W. L. *Graph representation learning*. Morgan & Claypool Publishers, 2020.

Hamilton, W. L., Ying, R., and Leskovec, J. Inductive representation learning on large graphs. In *Proceedings of the 31st International Conference on Neural Information Processing Systems*, pp. 1025–1035, 2017.

Horn, R. A. and Johnson, C. R. *Matrix analysis*. Cambridge university press, 2012.

Kipf, T. N. and Welling, M. Semi-supervised classification with graph convolutional networks. In *International Conference on Learning Representations (ICLR)*, 2017.

Klicpera, J., Bojchevski, A., and Günnemann, S. Predict then propagate: Graph neural networks meet personalized pagerank. In *International Conference on Learning Representations (ICLR)*, 2019.

Li, Y. and Zhang, Z.-L. Digraph laplacian and the degree of asymmetry. *Internet Mathematics*, 8(4): 381–401, 2012.

Ming Chen, Z. W., Zengfeng Huang, B. D., and Li, Y. Simple and deep graph convolutional networks. 2020.

Page, L., Brin, S., Motwani, R., and Winograd, T. The pagerank citation ranking: Bringing order to the web. Technical report, Stanford InfoLab, 1999.

Pei, H., Wei, B., Chang, K. C.-C., Lei, Y., and Yang, B. Geom-gcn: Geometric graph convolutional networks. In *International Conference on Learning Representations*, 2019.

Qiu, R., Yin, H., Huang, Z., and Chen, T. Gag: Global attributed graph neural network for streaming session-based recommendation. In *Proceedings of the 43rd International ACM SIGIR Conference on Research and Development in Information Retrieval*, pp. 669–678, 2020.

Rossi, E., Charpentier, B., Giovanni, F. D., Frasca, F., Günemann, S., and Bronstein, M. M. Edge directionality improves learning on heterophilic graphs. In *The Second Learning on Graphs Conference*, 2023. URL <https://openreview.net/forum?id=T4LRbAMWFn>.

Rozemberczki, B., Allen, C., and Sarkar, R. Multi-scale attributed node embedding. *Journal of Complex Networks*, 9(2):cnab014, 2021.

Sen, P., Namata, G., Bilgic, M., Getoor, L., Galligher, B., and Eliassi-Rad, T. Collective classification in network data. *AI magazine*, 29(3):93–93, 2008.

Shchur, O., Mumme, M., Bojchevski, A., and Günemann, S. Pitfalls of graph neural network evaluation. *arXiv preprint arXiv:1811.05868*, 2018.

Shuman, D. I., Narang, S. K., Frossard, P., Ortega, A., and Vandergheynst, P. The emerging field of signal processing on graphs: Extending high-dimensional data analysis to networks and other irregular domains. *IEEE signal processing magazine*, 30(3):83–98, 2013.

Singh, R., Chakraborty, A., and Manoj, B. Graph fourier transform based on directed laplacian. In *2016 International Conference on Signal Processing and Communications (SPCOM)*, pp. 1–5. IEEE, 2016.

Tong, Z., Liang, Y., Sun, C., Li, X., Rosenblum, D., and Lim, A. Digraph inception convolutional networks. *Advances in neural information processing systems*, 33, 2020a.

Tong, Z., Liang, Y., Sun, C., Rosenblum, D. S., and Lim, A. Directed graph convolutional network. *arXiv preprint arXiv:2004.13970*, 2020b.

Tong, Z., Liang, Y., Ding, H., Dai, Y., Li, X., and Wang, C. Directed graph contrastive learning. *Advances in neural information processing systems*, 34:19580–19593, 2021.

Topping, J., Di Giovanni, F., Chamberlain, B. P., Dong, X., and Bronstein, M. M. Understanding over-squashing and bottlenecks on graphs via curvature. 2022.

Veličković, P., Cucurull, G., Casanova, A., Romero, A., Liò, P., and Bengio, Y. Graph Attention Networks. *International Conference on Learning Representations*, 2018. URL <https://openreview.net/forum?id=rJXMpikCZ>. accepted as poster.

Wu, F., Souza, A., Zhang, T., Fifty, C., Yu, T., and Weinberger, K. Simplifying graph convolutional networks. In *International conference on machine learning*, pp. 6861–6871. PMLR, 2019.

Xu, K., Li, C., Tian, Y., Sonobe, T., Kawarabayashi, K.-i., and Jegelka, S. Representation learning on graphs with jumping knowledge networks. In *International conference on machine learning*, pp. 5453–5462. PMLR, 2018.

Zhang, X., He, Y., Brugnone, N., Perlmutter, M., and Hirn, M. Magnet: A neural network for directed graphs. *Advances in neural information processing systems*, 34:27003–27015, 2021.

Zhu, J., Yan, Y., Zhao, L., Heimann, M., Akoglu, L., and Koutra, D. Beyond homophily in graph neural networks: Current limitations and effective designs. *Advances in Neural Information Processing Systems*, 33, 2020.

A Proofs and Derivations

A.1 Derivation of DiLap T

Since the digraph is unweighted, then $\mathbf{P}_{ij} = \frac{1}{d_i^{\text{out}}}$ and $\frac{1}{d_i^{\text{out}}} \mathbf{A}_{i,:} = \mathbf{P}_{i,:}$. We have:

$$\begin{aligned}
(\mathbf{T}s)_i &= \sum_{v_j \in \mathcal{N}_i^{\text{out}}} \mathbf{P}_{ij}(s_i - s_j) \\
&= \frac{1}{d_i^{\text{out}}} s_i - \frac{1}{d_i^{\text{out}}} \sum_{v_j \in \mathcal{N}_i^{\text{out}}} s_j \\
&= (\mathbf{D}^{-1}s)_i - \frac{1}{d_i^{\text{out}}} \mathbf{A}_{i,:} s \\
&= (\mathbf{D}^{-1}s)_i - (\mathbf{P}s)_i \\
&= ((\mathbf{D}^{-1} - \mathbf{P})s)_i.
\end{aligned} \tag{12}$$

Thus, DiLap T can be represented as $\mathbf{D}^{-1} - \mathbf{P}$.

A.2 Proof of Lemma 4.1

Proof. Since the transition matrix $\tilde{\mathbf{P}}$ is row-stochastic, it follows that $\tilde{\mathbf{P}}^t \mathbf{J} = \mathbf{J}$. In light of Eq. (2) and considering that π is stochastic, we have $\mathbf{ZJ} = \mathbf{0}_{n \times n}$. Let $\mathcal{K} = \tilde{\mathbf{\Pi}}^{-\frac{1}{2}} \tilde{\mathcal{T}} \tilde{\mathbf{\Pi}}^{-\frac{1}{2}} = \tilde{\mathbf{\Pi}}^{\frac{1}{2}} (\tilde{\mathbf{D}}^{-1} - \tilde{\mathbf{P}}) \tilde{\mathbf{\Pi}}^{-\frac{1}{2}}$, $\mathcal{J} = \tilde{\mathbf{\Pi}}^{\frac{1}{2}} \mathbf{J} \tilde{\mathbf{\Pi}}^{\frac{1}{2}}$, and $\mathcal{Z} = \tilde{\mathbf{\Pi}}^{\frac{1}{2}} \mathbf{Z} \tilde{\mathbf{\Pi}}^{-\frac{1}{2}}$, incorporating these into Eq. (3), we have:

$$\mathcal{Z} + \mathcal{J} = (\mathcal{K} + \mathcal{J} - \tilde{\mathbf{D}}^{-1} + \mathbf{I})^{-1}. \tag{13}$$

By post-multiplying Eq. (13) from the right by $(\mathcal{K} + \mathcal{J} - \tilde{\mathbf{D}}^{-1} + \mathbf{I})$, we have:

$$\begin{aligned}
\mathbf{I} &= (\mathcal{Z} + \mathcal{J})(\mathcal{K} + \mathcal{J} - \tilde{\mathbf{D}}_c^{-1} + \mathbf{I}) \\
&= \mathcal{Z}\mathcal{K} + \mathcal{Z}\mathcal{J} - \mathcal{Z}\tilde{\mathbf{D}}^{-1} + \mathcal{Z} + \mathcal{J}\mathcal{K} + \mathcal{J}^2 - \mathcal{J}\tilde{\mathbf{D}}^{-1} + \mathcal{J}.
\end{aligned} \tag{14}$$

Since $\mathcal{J}^2 = \mathcal{J}$, $\mathcal{J}\mathcal{K} = \mathcal{J}(\tilde{\mathbf{D}}^{-1} - \mathbf{I})$, and $\mathcal{Z}\mathcal{J} = \tilde{\mathbf{\Pi}}^{\frac{1}{2}} \mathbf{Z} \tilde{\mathbf{\Pi}}^{\frac{1}{2}} = \mathbf{0}_{n \times n}$, Eq. (14) can be simplified to:

$$\mathcal{Z}(\mathcal{K} - \tilde{\mathbf{D}}^{-1} + \mathbf{I}) = \mathbf{I} - \mathcal{J}. \tag{15}$$

Similarly, by multiplying from the left, we establish that $(\mathcal{K} - \tilde{\mathbf{D}}^{-1} + \mathbf{I})\mathcal{Z} = \mathbf{I} - \mathcal{J}$. As $\pi^\top \mathbf{Z} = \mathbf{0}$, we have $\mathcal{J}\mathcal{Z} = 0$. Thus, $\mathcal{Z}(\mathcal{K} - \tilde{\mathbf{D}}^{-1} + \mathbf{I})\mathcal{Z} = \mathcal{Z}$. Furthermore, it can be straightforwardly inferred that $(\mathcal{K} - \tilde{\mathbf{D}}^{-1} + \mathbf{I})\mathcal{J} = 0$, then have $(\mathcal{K} - \tilde{\mathbf{D}}^{-1} + \mathbf{I})\mathcal{Z}(\mathcal{K} - \tilde{\mathbf{D}}^{-1} + \mathbf{I}) = (\mathcal{K} - \tilde{\mathbf{D}}^{-1} + \mathbf{I})$. Besides, considering the symmetry of the left part of Eq. (15), we have $(\mathcal{Z}(\mathcal{K} - \tilde{\mathbf{D}}^{-1} + \mathbf{I}))^\top = \mathcal{Z}(\mathcal{K} - \tilde{\mathbf{D}}^{-1} + \mathbf{I})$. Similarly, $((\mathcal{K} - \tilde{\mathbf{D}}^{-1} + \mathbf{I})\mathcal{Z})^\top = (\mathcal{K} - \tilde{\mathbf{D}}^{-1} + \mathbf{I})\mathcal{Z}$. These derivations satisfy the sufficient conditions for the Moore–Penrose pseudoinverse, such that

$$\mathcal{Z} = (\mathcal{K} - \tilde{\mathbf{D}}^{-1} + \mathbf{I})^\dagger. \tag{16}$$

Finally, recovering \mathcal{Z} and \mathcal{K} , which concludes the proof. \square

A.3 SVD for \mathcal{R}^\dagger

Given a matrix $\mathcal{R} \in \mathbb{R}^{N \times N}$, its Moore–Penrose pseudoinverse can be directly computed with an SVD-based method. Specifically, we first perform truncated SVD on $\mathcal{R} = \tilde{\mathbf{\Pi}}^{-\frac{1}{2}} \tilde{\mathcal{T}} \tilde{\mathbf{\Pi}}^{-\frac{1}{2}} - \tilde{\mathbf{D}}^{-1} + \mathbf{I} \approx \mathbf{U}_q \Sigma_q \mathbf{V}_q^\top$, where $\mathbf{U}_q \in \mathbb{R}^{N \times q}$ and $\mathbf{V}_q \in \mathbb{R}^{N \times q}$ contains the first q columns of \mathbf{U} and \mathbf{V} . $\Sigma_q \in \mathbb{R}^{q \times q}$ is the diagonal matrix of q largest singular values. It is a q -rank approximation of \mathcal{R} , which holds that $\text{rank}(\mathcal{R}) = q$. Then the Moore–Penrose pseudoinverse of \mathcal{R} can be easily computed as follows:

$$\mathcal{R}^\dagger = \mathbf{U}_q \Sigma_q^{-1} \mathbf{V}_q^\top. \tag{17}$$

To leverage sparsity of \mathcal{R} to avoid $\mathcal{O}(N^3)$ complexity, we adopt the randomized SVD algorithm proposed by (Halko et al., 2011; Cai et al., 2023) to first approximate the range of the input matrix with a low-rank orthonormal matrix, and then perform SVD on this smaller matrix:

$$\hat{\mathbf{U}}_q, \hat{\Sigma}_q, \hat{\mathbf{V}}_q^\top = \text{ApproxSVD}(\mathcal{R}, q), \quad \hat{\mathcal{R}}_{\text{SVD}} = \hat{\mathbf{U}}_q \hat{\Sigma}_q \hat{\mathbf{V}}_q^\top, \tag{18}$$

where $\hat{\mathbf{U}}_q$, $\hat{\Sigma}_q$, and $\hat{\mathbf{V}}_q$ are the approximated versions of \mathbf{U}_q , Σ_q , and \mathbf{V}_q . Then the Moore-Penrose pseudoinverse of \mathcal{R} can be computed by:

$$\mathcal{R}^\dagger = \hat{\mathbf{U}}_q \hat{\Sigma}_q^{-1} \hat{\mathbf{V}}_q^\top. \quad (19)$$

The computation cost of randomized truncated SVD takes $\mathcal{O}(qK)$, where K is the number of non-zero elements in \mathcal{R} , so we have $K = |E|$. Thus, the sparsity degree of \mathcal{R} can determine the time complexity of its Moore-Penrose pseudoinverse, which demonstrates the importance of Lemma 4.1.

B Pseudo Code for CGNN

Algorithm 1 CGNN

Input: Digraph $G = (V, E, \mathbf{X})$; Depth L ; Hidden size d' ; Number of classes K

Output: Logits $\hat{Y} \in \mathbb{R}^{N \times K}$

- 1: Compute the anchor \mathbf{a} and node-anchor similarities to construct G' with Eq. (7).
- 2: Add all edges from G' to G to generate \tilde{G} .
- 3: Compute the Weight DiLap $\tilde{\mathcal{T}}$ for \tilde{G} with Eq. (6).
- 4: Compute \mathcal{R} and its Moore-Penrose pseudoinverse with Eq. (8) and Eq. (19).
- 5: Compute the commute time matrix \mathcal{C} with Eq. (10).
- 6: Compute the normalized proximity matrix $\tilde{\mathcal{C}}$ with $\tilde{\mathcal{C}}^{\text{out}} = \mathbf{A} \odot \tilde{\mathcal{C}}$ and $\tilde{\mathcal{C}}^{\text{in}} = \mathbf{A}^\top \odot \tilde{\mathcal{C}}$.
- 7: **for** $\ell \in \{1, \dots, L\}$ **do**
- 8: Layer-wise message passing with Eq. (11).
- 9: **end for**
- 10: $\mathbf{H} = \text{MLP}(\mathbf{H}^{(L)})$.
- 11: $\hat{Y} = \text{Softmax}(\mathbf{H})$.

Complexity Analysis The time complexity of randomized truncated SVD to compute \mathcal{R}^\dagger is $\mathcal{O}(q|E|)$, and the message passing iteration has the same time complexity as GraphSAGE with $\mathcal{O}(|E|)$. Therefore, the overall time complexity of CGNN is $\mathcal{O}(q|E|)$.

C Implementation Details

C.1 Experimental Settings

We evaluate the performance by node classification accuracy with standard deviation in the semi-supervised setting. For Squirrel and Chameleon, we use 10 public splits (48%/32%/20% for training/validation/testing) provided by (Pei et al., 2019). For the remaining datasets, we adopt the same splits as (Tong et al., 2020a, 2021), which chooses 20 nodes per class for the training set, 500 for the validation set, and allocates the rest to the test set. We conduct our experiments on 2 Intel Xeon Gold 5215 CPUs and 1 NVIDIA GeForce RTX 3090 GPU.

C.2 Data Statistics

The dataset used in Section 5 are Squirrel, Chameleon (Rozemberczki et al., 2021), Citeseer (Sen et al., 2008), CoraML (Bojchevski & Günnemann, 2017), and AM-Photo (Shehur et al., 2018). We summarize their statistics in Table 4. `homo_ratio` represents the homophily ratio, a metric proposed by Zhu et al. (2020), which is employed to gauge the degree of homophily within the graph. A lower `homo_ratio` signifies a greater degree of heterophily, indicating a higher prevalence of edges that connect nodes of differing classes.

C.3 Hyperparameter Settings

For our model, we tune the hyperparameters based on the highest average validation accuracy. We utilize the randomized truncated SVD algorithm for computing the Moore-Penrose pseudoinverse of matrix \mathcal{R} , setting the required rank q to 5 for all datasets. The learning rate lr is selected from

Table 4: Statistics of the datasets.

Dataset	N	$ E $	# Feat.	# Classes	homo_ratio
Squirrel	5,201	217,073	2,089	5	0.22
Chameleon	2,277	36,101	2,325	5	0.23
Cora-ML	2,995	8,416	2,879	7	0.79
Citeseer	3,312	4,715	3,703	6	0.74
AM-Photo	7,650	238,162	745	8	0.83

$\{0.01, 0.005\}$, and the weight decay wd from $\{0, 5e-5, 5e-4\}$. In the model architecture, the number of layers L vary among $\{1, 2, 3, 4, 5\}$ and the dimension d' is selected from $\{32, 64, 128, 256, 512\}$. The comprehensive hyperparameter configurations for CGNN are detailed in Table 5.

Table 5: Hyperparameters specifications.

Dataset	lr	wd	L	d'
Squirrel	0.005	0	5	128
Chameleon	0.01	0	4	128
CoraML	0.01	0	2	64
Citeseer	0.01	0	2	128
AM-Photo	0.005	0	2	512

D Additional Experiments

D.1 Link Prediction

For link prediction, we compare our method with all baselines on Citeseer and CoraML datasets. Our experimental setup follows the protocol established by (Zhang et al., 2021), considering two distinct types of link prediction tasks for performance evaluation. The first task involves predicting the direction of edges between pairs of nodes, while the second focuses on predicting the existence of edges. For both tasks, we partition the data by removing 15% of the edges for testing and 5% for validation, with the remaining edges used for training. The results, detailed in Table 6, reveal that CGNN excels in the direction prediction task. Meanwhile, in the edge existence prediction task, MagNet yields the best results, with CGNN also achieving comparable performance. These findings show CGNN’s effectiveness in accurately capturing directed structural patterns in graphs.

D.2 Sensitivity analysis

We investigate the sensitivity of CGNN to key hyperparameters that influence its performance, specifically focusing on the number of layers L and the dimension of the hidden layer d' . We explore a range of values for L , considering $\{1, 2, 3, 4, 5\}$, and for d' , considering $\{32, 64, 128, 256, 512\}$. From Fig. 5, we observe that we observe that CGNN achieves optimal performance with $L = 5$ and $d' = 128$ on Squirrel, and with $L = 2$ and $d' = 64$ on CoraML. This suggests that deeper models are necessary to effectively aggregate valuable information in heterophilic graphs, whereas in homophilic graphs, leveraging local neighborhood information is generally adequate.

Table 6: Link prediction results.

Method	Direction prediction		Existence prediction	
	Citeseer	CoraML	Citeseer	CoraML
GCN	77.69 ± 0.73	75.68 ± 0.97	70.27 ± 2.12	80.67 ± 1.08
GAT	76.09 ± 0.09	50.02 ± 0.05	50.82 ± 0.36	50.00 ± 0.01
GraphSAGE	75.16 ± 0.91	70.07 ± 1.43	70.59 ± 1.74	69.32 ± 0.58
APPNP	79.23 ± 0.35	78.64 ± 0.70	81.14 ± 1.21	85.46 ± 0.80
MixHop	79.40 ± 0.42	78.62 ± 1.25	80.11 ± 1.93	85.21 ± 0.90
GPRGNN	79.15 ± 0.35	77.88 ± 1.30	78.15 ± 0.24	83.83 ± 0.74
GCNII	78.60 ± 0.69	75.51 ± 1.90	79.48 ± 1.74	75.51 ± 1.90
DGCN	82.38 ± 0.55	74.13 ± 1.07	81.11 ± 2.28	80.30 ± 1.25
DiGCN	83.06 ± 0.70	74.92 ± 0.88	85.08 ± 1.26	81.06 ± 1.16
MagNet	79.36 ± 0.44	77.71 ± 1.04	88.20 ± 1.05	87.21 ± 0.72
DiGCL	81.89 ± 0.76	76.05 ± 0.97	82.96 ± 1.32	84.23 ± 1.26
DirGNN	82.09 ± 0.88	77.93 ± 0.76	85.18 ± 1.02	83.37 ± 1.83
CGNN	84.97 ± 0.71	80.33 ± 0.90	85.27 ± 1.30	82.08 ± 1.22

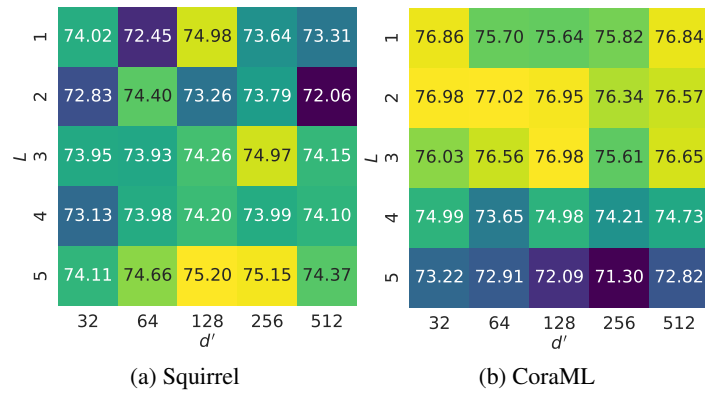


Figure 5: Sensitivity analysis on Squirrel and CoraML.